Supplementary Materials

Exploring nebular ingassing in the inner Solar System: evidence from the unique achondrite NWA 8409

Stephant A.[1,2], Desch S.J.[3], Anand, M.[2,4], Zhao X.[2], Cuppone T.[5], Rider-Stokes B.G.[2], Gamblin J.[6], Füri E.[6], Nottingham M.[7], Carli C.[1], Pratesi G.[5] & Franchi, I. A.[2]

[1]IAPS-INAF, Rome, Italy.
[2]School of Physical Sciences, The Open University, Milton Keynes, UK.
[3]School of Earth and Space Exploration, Arizona State University, USA.
[4]Department of Mineralogy, The Natural History Museum, London, UK.
[5]Department of Earth Sciences, University of Florence, Italy.
[6]Université de Lorraine, CNRS, CRPG, F-54000 Nancy, France.
[7]School of Geographical and Earth Sciences, University of Glasgow,

This file includes:
Supplementary text
Figures S1 to S9
Table S1

Supplementary text

1. Methods

1.1. SEM-EPMA

Preliminary petrographical and mineralogical characterization throughout Secondary Ion Microscope (SEM) imaging, as well as semi-quantitative micro-chemical analyses, were obtained at MEMA (Centro Servizi di Microscopia Elettronica e Microanalisi) at the University of Florence using a S3/11/26 5:54:00 AMEM-EDS electronic microscope (ZEISS EVO MA 15) equipped with an EDS/SDD analytical system, an Oxford Ultimax 40 detector and the Aztec 5.0 SP1 software. The measurements were performed with the following operative conditions: an acceleration potential of 15 kV; 500 pA beam current; working distance comprised between 8.5-9.0 mm; 20s live time as acquisition rate useful to archive at least 600.000 cts; on Co standard, process time 4 for point analyses; 500 μs pixel dwell time for maps acquisition with 1024x768 pixel resolution. The software used for the microanalysis (Aztec 5.0 SP1) employs the XPP matrix correction scheme. This is a Phi-Rho-Z approach which uses exponentials to describe the shape of the φ (ρz) curve. XPP matrix correction was chosen because of its favorable performance in situations of severe absorption such as the analysis of light elements in a heavy matrix. The procedure is a "standard-less" quantitative analysis that employs pre-acquired standard materials for calculations and the monitoring of constant analytical

conditions (i.e., filament emission) is archived with repeated analyses of a Co metallic standard. Modal abundances were estimated using SEM-BSE images and relative X-ray elemental maps in conjunction with Adobe Photoshop(R) and Fiji program, an open-source image processing package based on ImageJ2 processing software (Schindelin et al., 2012). Modes were obtained using a black/white contrast thresh-holding method where thresholds were selected based on knowledge of the mineral phases in the sample (with the aim of X-ray elemental maps). Back-scattered image of the NWA 8409 chip with modal abundance is presented in Figure S1.

Chemical characterization of silicates and sulfides on NWA 8409 chip were carried out at the joined laboratory (LaMA, Laboratorio MicroAnalisi) of the Earth Sciences Department of the University of Firenze (DST) and the National Council of Research - Institute of Geosciences and Earth Resources (CNR-IGG) of Firenze (Italy). The e probe micro-analyser (EPMA) used is a JEOL Superprobe JXA-8230, equipped with 5 wavelength dispersion spectrometers (WDS) operating with different analyzer crystals and different detectors (gas flow and sealed Xe type). For silicates, oxides and phosphates, the working conditions used were 15 kV accelerating voltage, beam current at 20 μA and beam diameter of 3 μm (for olivines and pyroxenes) and 5 μm for feldspar to reduce diffusion effect on alkali, and sulfides. Variable counting times were set for major and minor elements: 15s on peak and 7s on both backgrounds for major and some minor elements; 30–40s on peak and 15–20s on both backgrounds for minor elements, except for Na that was measured for 10s on peak and 5s on background, to limit the alkali loss. The acquisition order was Si, Na, K, Cl and Fe, followed by Mg, Ca, Mn, F, S and Al, Ti and P. For sulfides the working conditions used were 20 kV accelerating voltage, beam current at 10 μA and beam diameter of 3-5 μm. Counting times were set with the same rationale of silicates. Silica is measured for check. A selection of natural and synthetic phases was used as primary standard for the elemental calibration (chalcopyrite for S and Cu, chalcopyrite or marcasite for Fe depending on the sulfide type, sphalerite for Zn, Astimex pentlandite for Ni, cobaltite for Co, pure metal for Ti, Cr and Mn Astimex albite for Si and Na, plagioclase for Al, olivine for Mg, diopside for Ca, sanidine for K, apatite for P, celestine for S, tugtupite for Cl, barite for Ba and Smithsonian ilmenite for Ti and Fe). Several natural mineral phases are used as secondary quality-control standards (olivine San Carlos, augite Kakanui, diopside Smithsonian, albite Astimex, plagioclase Astimex, ilmenite and chromite Smithsonian, apatite Astimex). The ZAF algorithm is used for matrix correction. The laboratory long term average of replicate measurements on secondary international reference standards shows a good precision with a variation coefficient lower than 1% for silica, up to 2% for the other major elements and up to 5% for minor elements. Accuracy is within 1% for major and most of minor elements and total R2 lower than 1 for all the analyzed standards.

1.2. ICP-MS

The determinations of bulk major and trace element compositions were performed at the Department of Earth Sciences, University of Firenze (Italy). Approximately 20 to 50 mg of whole rock powder were totally digested in pre-cleaned PFA Savillex beakers with a mixture of concentrated HF and HNO_3 (4:1) for 48h at 150°C. The solutions were then dried down at 140°C and refluxed with concentrated HNO_3 twice. After this step, samples were evaporated

and dissolved in aqua regia solution (HCl- HNO_3) and refluxed for 72h at 150°C to achieve complete dissolution of the more refractory phases. Once dried down, samples were dissolved in HCl 6M and refluxed for 48h at 150°C and then evaporated to complete dryness. Few drops of concentrated HNO_3 were then added to ensure the complete removal of chlorides for the following measurement through ICP-MS. Samples were then diluted in 7M HNO_3 and MilliQ to reach the desired elemental concentrations for ICP-MS analysis in 2% HNO_3. The analyses were performed with an Agilent 7800 ICP-MS using Re-Rh as internal standards and different multi-elemental standard solutions for calibration (Inorganic Ventures, VA, USA) conveniently diluted for the concentration ranges tolerated by the instrument. Accuracy and precision, calculated on the basis of repeated analyses of samples (Allende CV, n=4) and rock standards (AGV-1, BHVO-1) were better than 5% for most of trace elements, and as a whole better than 10% for all the analyzed elements of the reference values (Jochum et al., 2005). REE pattern of NWA 8409 and its paired NWA 7325 and NWA 8486 are presented in Figure S5, as well as the bulk chemistry in Figure S6 and data are shown in Table S2.

1.3. EBSD

For petrographic examination, the small chip of NWA 8409 was removed from indium and embedded within a 1-inch round epoxy mount, polished using a Vibromet vibratory polisher, and carbon-coated (< 5 μm) using a Safematic CCU-010 Compact Coating Unit. The mount was investigated using a Zeiss Crossbeam 550 at The Open University fitted with an Oxford Instruments Symmetry 2 Electron Back-Scattered Detector (EBSD). High-resolution element maps were collected by Energy Dispersive X-Ray Spectroscopy (EDS) using the Oxford Instruments Ultim Extreme and Oxford Instruments Ultim Max detectors, also fitted to the Zeiss Crossbeam 550. The sample was tilted to 70° and a 20 kV, 1.5–2 nA electron beam was used to generate EBSD "maps," consisting of electron backscatter diffraction patterns (EBSP) acquired at step sizes of 0.1–1 μm and a working distance of 10 mm. Data were processed offline using Aztec Crystal, where a "wildspike" correction and noise reduction (level 8) were applied. Structural characterization of diopside and forsterite are presented in Figure S4.

2. Bulk water content estimation

Our estimation of the NWA 8409 parent body bulk water content is limited to (i) our knowledge of the formation scenario of the rock and (ii) the partition coefficient of hydrogen between melt and NAMs. Frossard et al. (2019) have estimated that NWA 8486 and NWA 7325, hence also NWA 8409, could have been formed by 20-50 % melting of a pyroxene-rich anorthosite, similar to the Apollo sample 62236. We used a simple single batch melting model similar to the one used for ureilites (Peterson et al., 2023), acapulcoites-lodranites (Stephant et al., 2023), eucrites (Stephant et al., 2021) and angrites (Rider-Stokes et al., 2024), following the equation:

$$C_0 = C_s \times \frac{(D + F(1 - D))}{D}$$

With C_0 and C_s the parent melt and pyroxene H_2O concentration, respectively, D the partition coefficient from Sarafian et al. (2019) estimated for 0.1 MPa, more adequate for asteroidal settings and F the percentage of partial melting. The water content estimated for the bulk parent body ranges from 8 μg/g H_2O for 20% partial melting to from 17 μg/g H_2O for 50% partial melting.

References

Barrat, J.A., Greenwood, R.C., Verchovsky, A.B., Gillet, Ph., Bollinger, C., Langlade, J.A., Liorzou, C., Franchi, I.A., 2015. Crustal differentiation in the early solar system: Clues from the unique achondrite Northwest Africa 7325 (NWA 7325). Geochimica et Cosmochimica Acta 168, 280–292. https://doi.org/10.1016/j.gca.2015.07.020

Frossard, P., Boyet, M., Bouvier, A., Hammouda, T., Monteux, J., 2019. Evidence for anorthositic crust formed on an inner solar system planetesimal. Geochem. Persp. Let. 28–32. https://doi.org/10.7185/geochemlet.1921

Harries, D., Zhao, X., Franchi, I., 2023. Upper limits of water contents in olivine and orthopyroxene of equilibrated chondrites and several achondrites. Meteorit & Planetary Scien 58, 705–721. https://doi.org/10.1111/maps.13980

Heber, V.S., Wieler, R., Baur, H., Olinger, C., Friedmann, T., Burnett, D.S., 2009. Noble gas composition of the solar wind as collected by the Genesis mission. Geochimica et Cosmochimica Acta. 10.1016/j.gca.2009.09.013

Jochum, K.P., Nohl, U., Herwig, K., Lammel, E., Stoll, B., Hofmann, A.W., 2005. GeoReM: A New Geochemical Database for Reference Materials and Isotopic Standards. Geostand Geoanalyt Res 29, 333–338. https://doi.org/10.1111/j.1751-908X.2005.tb00904.x

Koga, K., Hauri, E., Hirschmann, M., Bell, D., 2003. Hydrogen concentration analyses using SIMS and FTIR: Comparison and calibration for nominally anhydrous minerals. Geochem Geophys Geosyst 4, 2002GC000378. https://doi.org/10.1029/2002GC000378

Kumamoto, K.M., Warren, J.M., Hauri, E.H., 2017. New SIMS reference materials for measuring water in upper mantle minerals. American Mineralogist 102, 537–547. https://doi.org/10.2138/am-2017-5863CCBYNCND

Leya, I., Masarik, J., 2009. Cosmogenic nuclides in stony meteorites revisited. Meteoritics & Planetary Science 1061–1086. 10.1111/j.1945-5100.2009.tb00788.x

Peterson, L.D., Newcombe, M.E., Alexander, C.M.O., Wang, J., Sarafian, A.R., Bischoff, A., Nielsen, S.G., 2023. The H2O content of the ureilite parent body. Geochimica et Cosmochimica Acta 340, 141–157. https://doi.org/10.1016/j.gca.2022.10.036

Rider-Stokes, B.G., Stephant, A., Anand, M., Franchi, I.A., Zhao, X., White, L.F., Yamaguchi, A., Greenwood, R.C., Jackson, S.L., 2024. Evidence against water delivery by impacts within 10 million years of planetesimal formation. Earth and Planetary Science Letters 642, 118860. https://doi.org/10.1016/j.epsl.2024.118860

Sarafian, A.R., Nielsen, S.G., Marschall, H.R., Gaetani, G.A., Righter, K., Berger, E.L., 2019. The water and fluorine content of 4 Vesta. Geochimica et Cosmochimica Acta 266, 568–581. https://doi.org/10.1016/j.gca.2019.08.023

Schindelin, J., Arganda-Carreras, I., Frise, E., Kaynig, V., Longair, M., Pietzsch, T., Preibisch, S., Rueden, C., Saalfeld, S., Schmid, B., Tinevez, J.-Y., White, D.J., Hartenstein, V., Eliceiri, K., Tomancak, P., Cardona, A., 2012. Fiji: an open-source platform for biological-image analysis. Nat Methods 9, 676–682. https://doi.org/10.1038/nmeth.2019

Stephant, A., Wadhwa, M., Hervig, R., Bose, M., Zhao, X., Barrett, T.J., Anand, M., Franchi, I.A., 2021. A deuterium-poor water reservoir in the asteroid 4 Vesta and the inner solar system. Geochimica et Cosmochimica Acta 297, 203–219. https://doi.org/10.1016/j.gca.2021.01.004

Stephant, A., Zhao, X., Anand, M., Davidson, J., Carli, C., Cuppone, T., Pratesi, G., Franchi, I.A., 2023. Hydrogen in acapulcoites and lodranites: A unique source of water for planetesimals in the inner Solar System. Earth and Planetary Science Letters 615, 118202. https://doi.org/10.1016/j.epsl.2023.118202

Supplementary figures

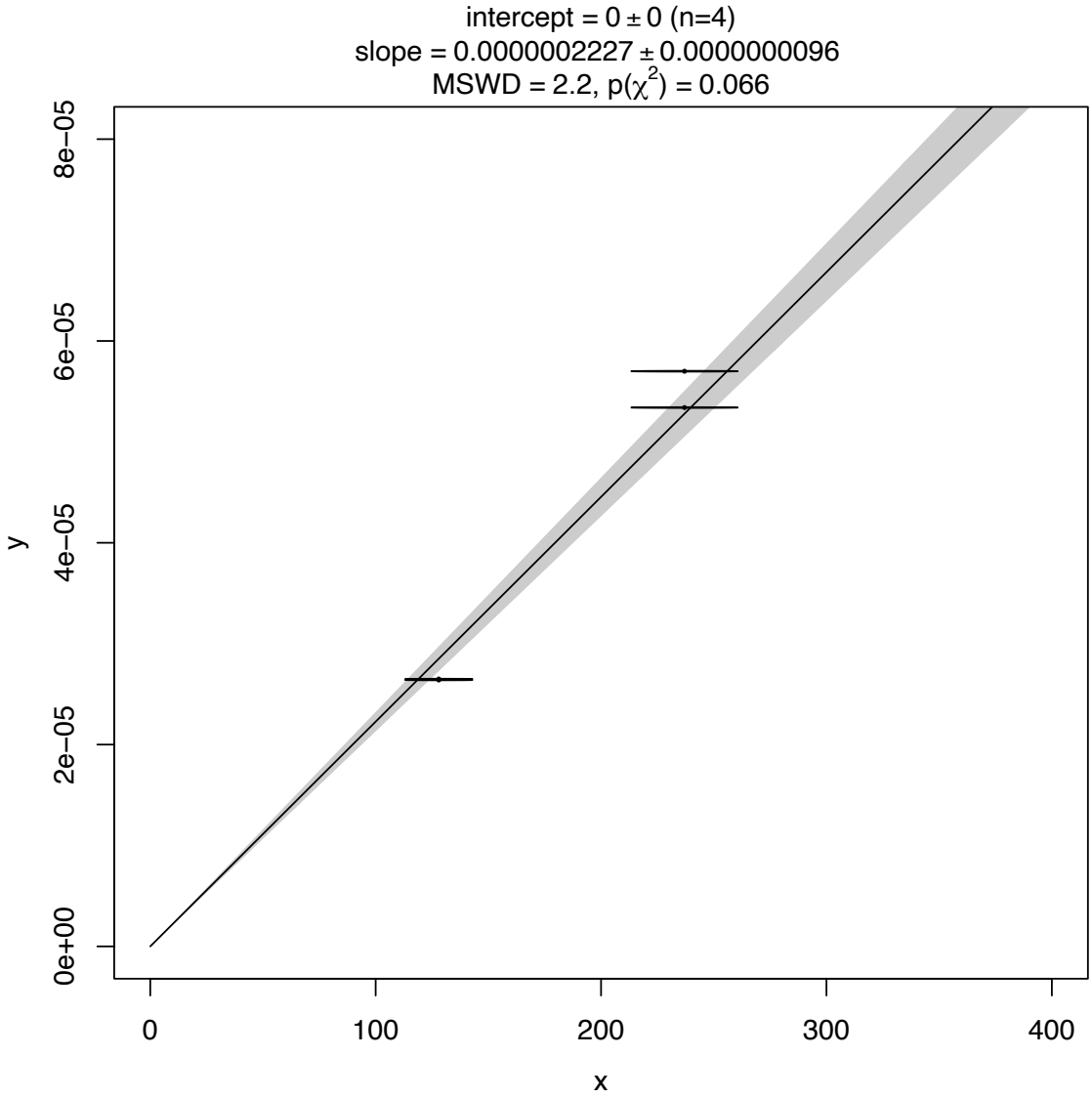

Figure S1 - Orthopyroxene regression line

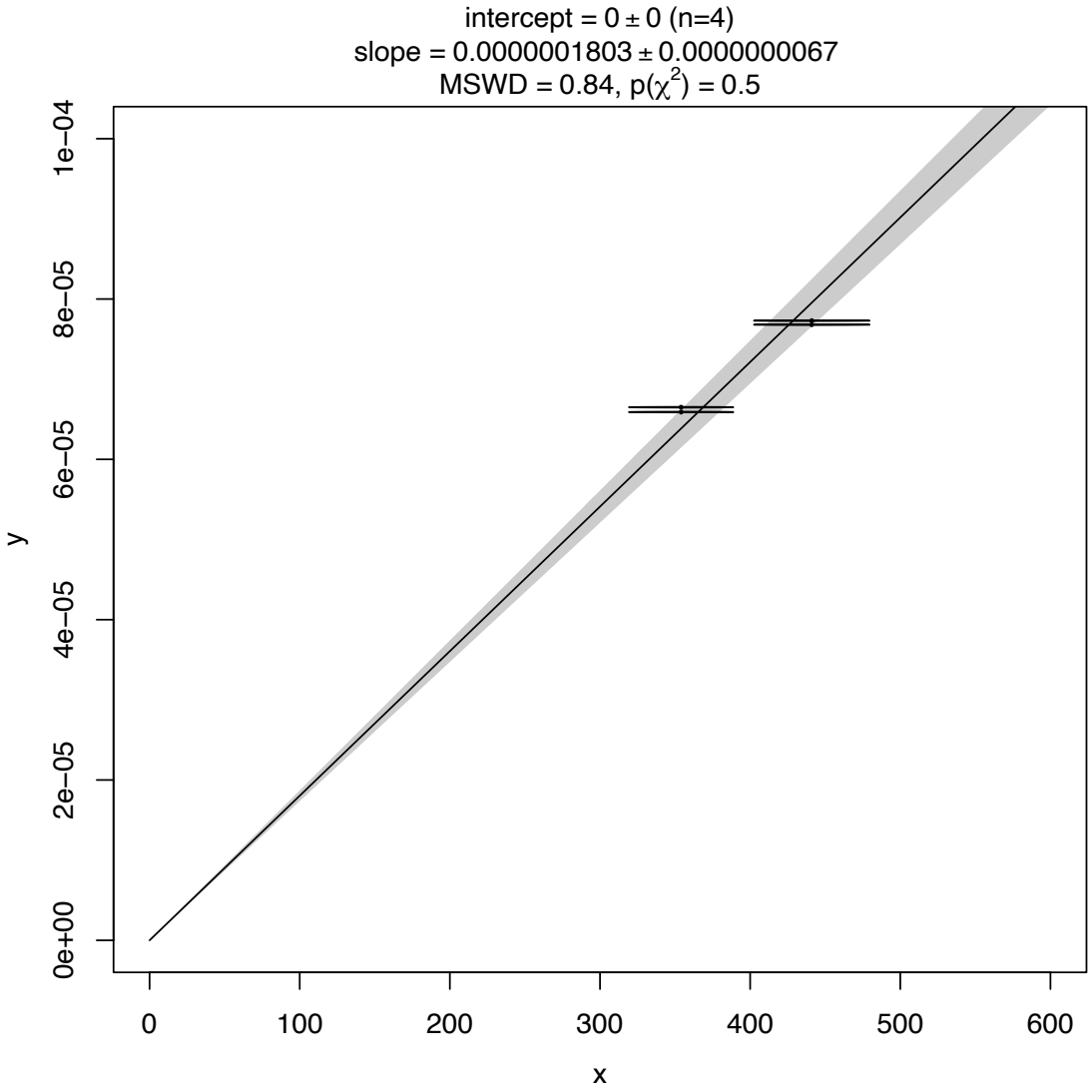

Figure S2- Clinopyroxene regression line

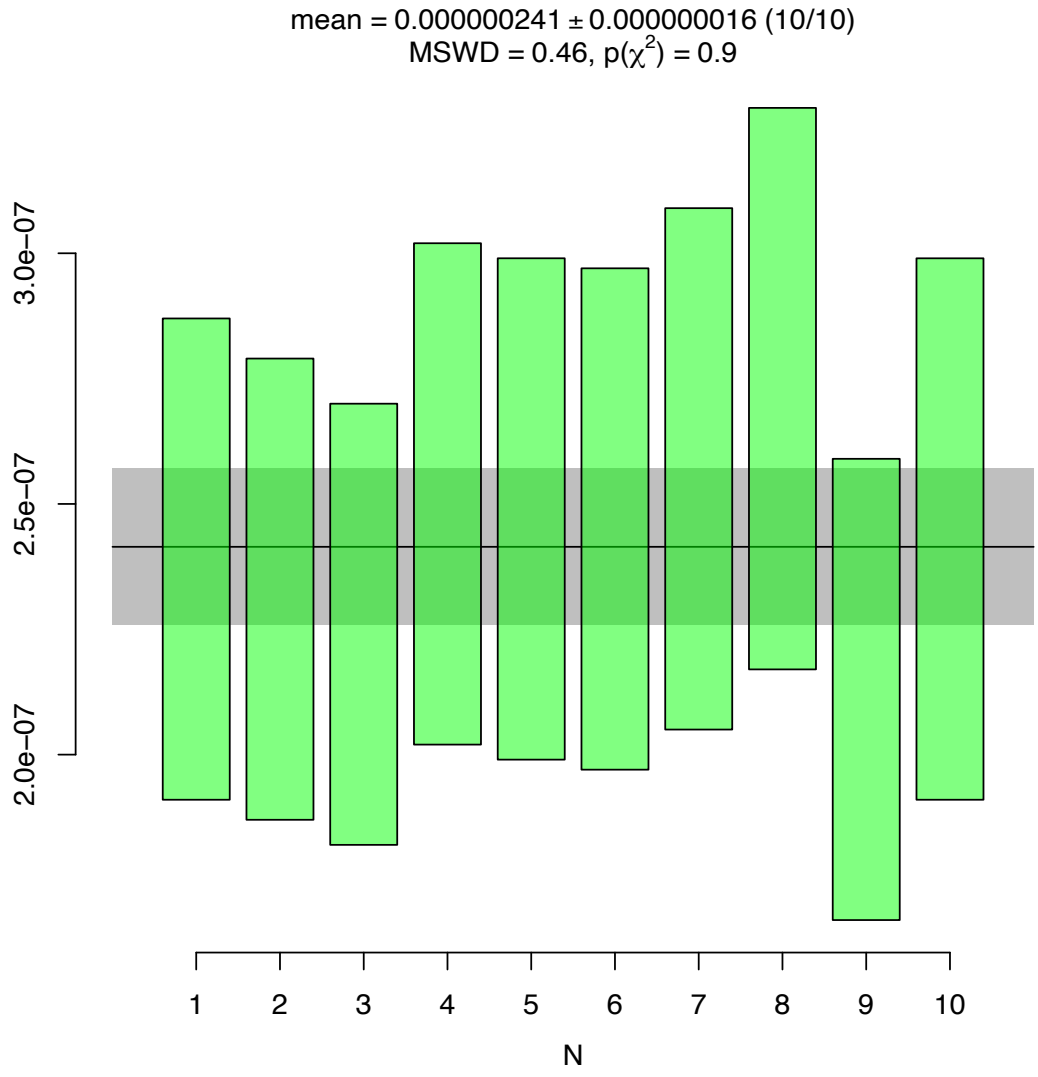

Figure S3 - SCOL H/^{16}O background estimation

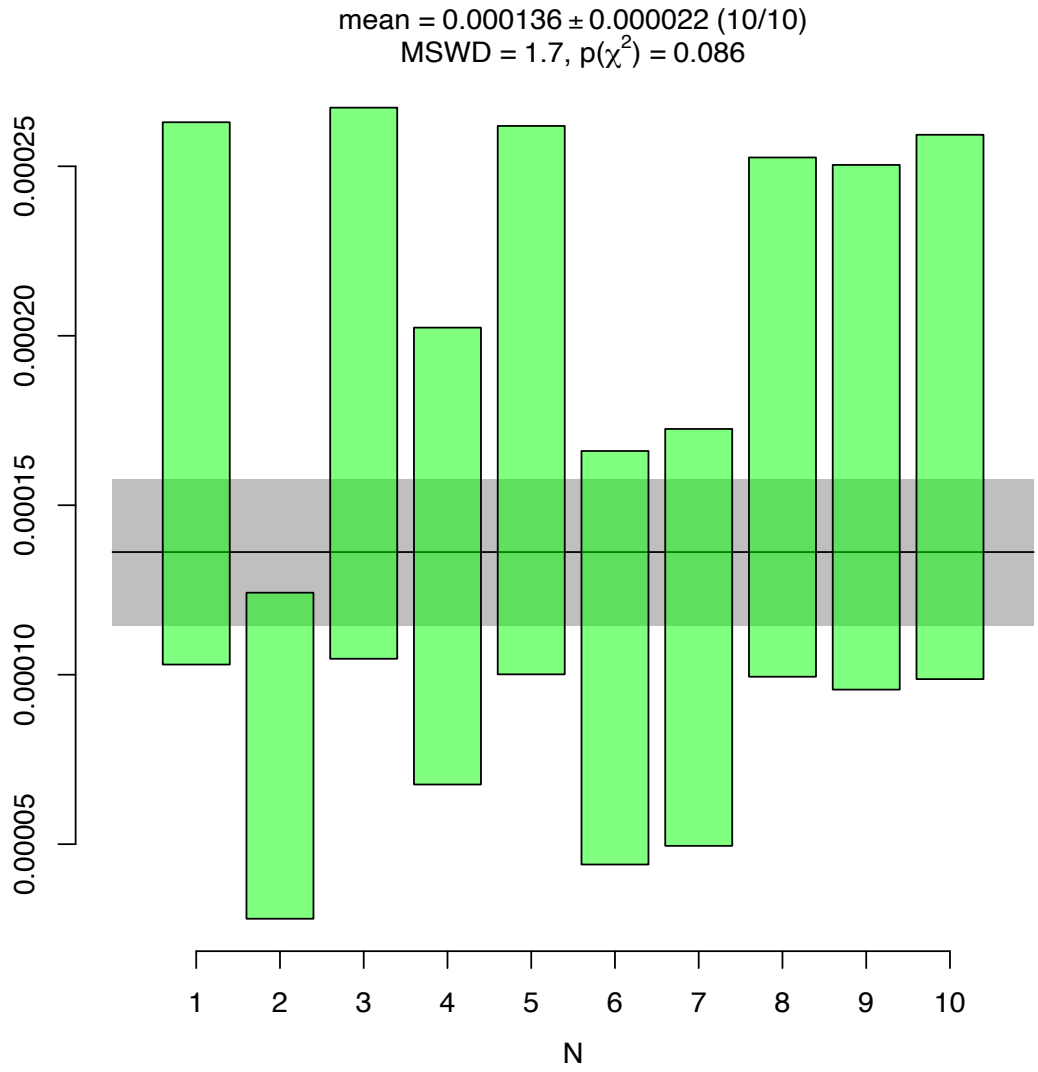

Figure S4 - SCOL D/H background estimation

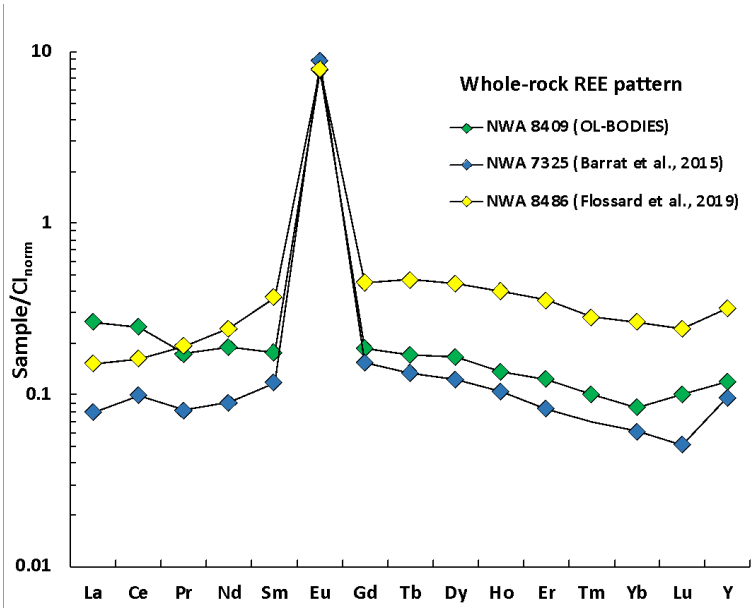

Figure S5 – REE pattern of NWA 8409 and its paired NWA 7325 and NWA 8486.

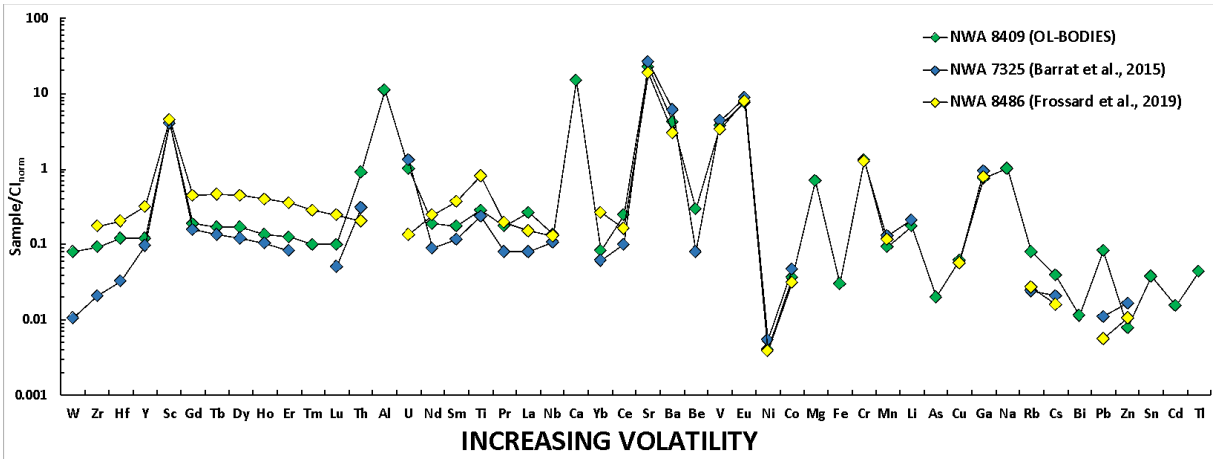

Figure S6 – Bulk composition of NWA 8409.

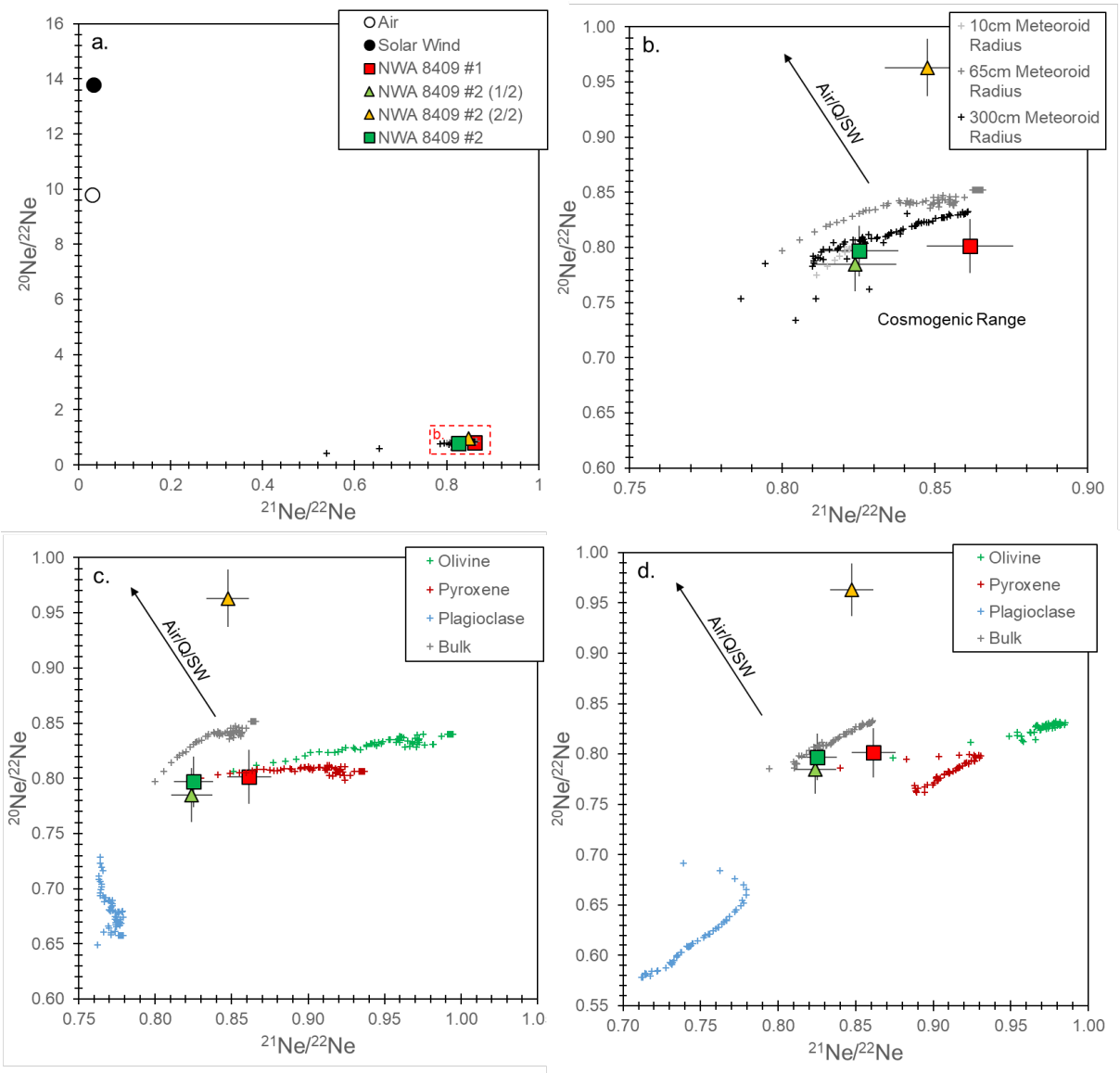

Figure S7 - Ne isotopic ratios for NWA 8409 (a.); also showing (b.)s, models for different meteoroid radii, adopting bulk sample chemistry; models for a meteoroid of 65 cm radius (c.), and 300 cm radius (d.), with chemistry based on end-member mineralogies measured within NWA 8409. Noble gas end member compositions: Solar wind (Heber et al., 2009); Cosmogenic (Leya and Masarik, 2009).

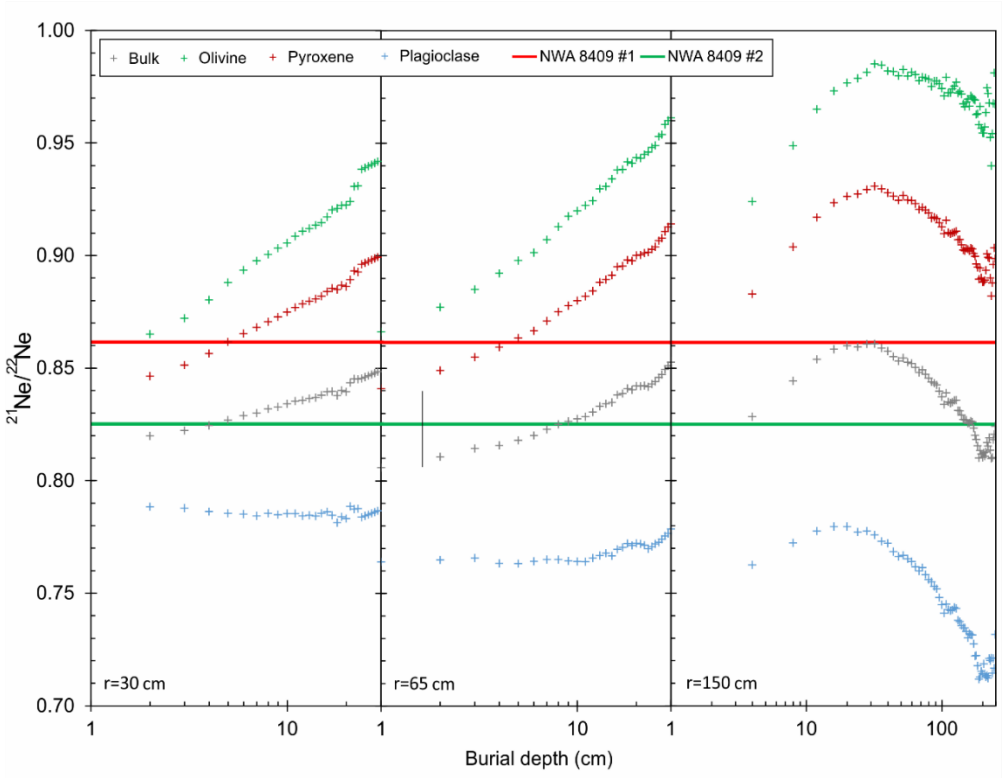

Figure S8 - Theoretical cosmogenic nuclide production rate curves for mineral separates and bulk rock chemistry compositions applied to the models of Leya and Masarik (2009). Shown are a range of meteoroid radii (indicated in the bottom left corner of each panel), with production rate ratios shown relative to the sample burial depth within the meteoroid. Note that the poor fit of both sample measurements (indicated as green and red horizontal lines) likely show aliquot chemistry heterogeneity.

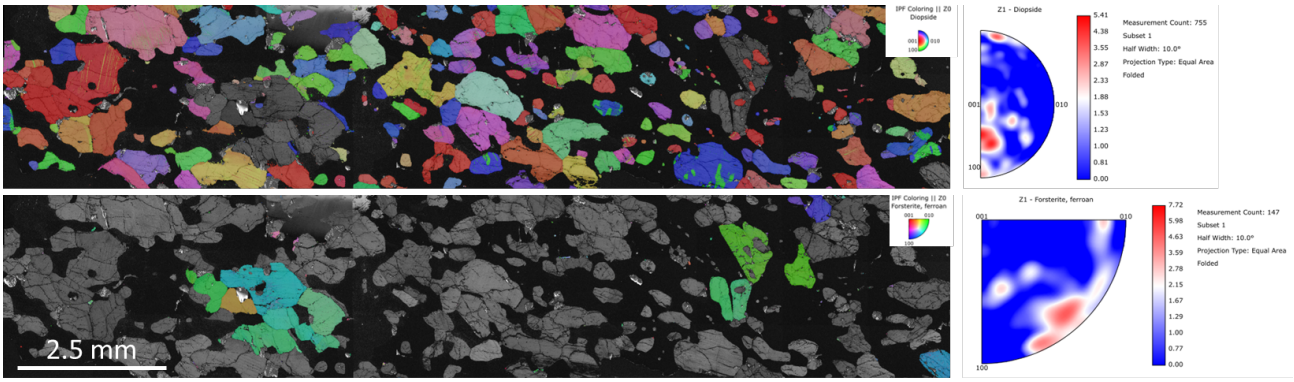

Fig. S9 – Structural characterization of diopside (a) and forsterite (b) in NWA 8409. The grain orientation is depicted by the IPF parallel to the Z0 axis.

Supplementary tables

Standards	H_2O (µg/g)	2σ	δD (‰)	2σ	References
KBH-1 (cpx)	186	-	-113	4	(Koga et al., 2003)
116610-21 (cpx)	354	28	-	-	(Kumamoto et al., 2017)
116610-15 (cpx)	441	31	-	-	(Kumamoto et al., 2017)
116610-18 (cpx)	199	13	-	-	(Kumamoto et al., 2017)
116610-10 (opx)	128	12	-	-	(Kumamoto et al., 2017)
116610-26 (opx)	237	19	-	-	(Kumamoto et al., 2017)
116610-29 (opx)	62	4	-	-	(Kumamoto et al., 2017)
San carlos (ol)	0.9	0.2	-	-	(Harries et al., 2023)

Table S1 – Terrestrial standards δD and H_2O contents